(15) S. Natelson, M. L. Scott, and C. Belfa, *Am. J. Clin. Pathol.*, **21**, 275 (1951).
(16) H. L. Conn, Jr., L. Wilds, and J. Helwig, *J. Clin. Invest.*, **33**, 732 (1954).
(17) A. Kleinzeller and J. H. Cort, *Biochem. J.*, **67**, 15 (1954).
(18) T. Fujita and M. Itakura, *J. Lab. Clin. Med.*, **92**, 135 (1978).
(19) C. Kobayashi, *Jikeikai Med. J.*, **89**, 46 (1974).
(20) L. E. Gol'dberg, *Antibiotiki*, **12**, 588 (1967).
(21) L. E. Gol'dberg and I. P. Belova, *Antibiotiki*, **13**, 1076 (1968).
(22) P. Hekman and C. A. M. van Ginneken *J. Pharmacokinet. Biopharm.*, **10**, 77 (1982).
(23) H. Akaike, *Math. Sci.*, **14** (153), 5 (1976).
(24) K. Yamaoka, T. Nakagawa, and T. Uno, *J. Pharmacokinet. Biopharm.*, **6**, 165 (1978).

Aqueous Conversion Kinetics and Mechanisms of Ancitabine, a Prodrug of the Antileukemic Agent Cytarabine

LEE E. KIRSCH * and ROBERT E. NOTARI ˣ

Received November 22, 1982 from *Lloyd M. Parks Hall, College of Pharmacy, The Ohio State University, Columbus, OH 43210.* Accepted for publication June 1, 1983. *Present address: Product Development Division, Eli Lilly and Co., Indianapolis, IN 46206.

Abstract □ The kinetics of conversion of the prodrug ancitabine to the anticancer drug cytarabine have been studied in aqueous solutions in the pH range of 1.5–10.7, temperature range of 19.5–80.0°C, ionic strength range of 10^{-4} to 1.5, and in the presence of several general-base catalysts. Under all conditions ancitabine was quantitatively converted to cytarabine. The pH–rate profiles were linear with slope = 1 in alkaline pH, becoming pH independent in the region of maximum stability at pH ≤ 4, where buffer catalysis was found to be insignificant and $k_{obs} \cong (1.12 \times 10^{11}\ h^{-1})\exp\{-10121\ deg/T\}$. At 30°C, pH ≤ 4, it is calculated that an aqueous ancitabine solution will maintain 90% of its initial concentration for 12 d. A novel method for measuring general-base catalysis in competition with predominating specific-base catalysis and in the presence of secondary salt effects at constant ionic strength was developed. Three mechanisms of hydrolytic prodrug conversion are proposed: nucleophilic hydroxide addition, general base-assisted nucleophilic water attack, and spontaneous water attack.

Keyphrases □ Ancitabine—conversion to cytarabine, kinetics, aqueous solutions □ Cytarabine—conversion of ancitabine, aqueous solutions, kinetics □ Kinetics—ancitabine conversion to cytarabine, aqueous solutions

Ancitabine (I), a prodrug of the antileukemic agent cytarabine (II), has been shown to be more effective than II in several animal tumor systems (1, 2) (Scheme I). The pharmacological activity of I is attributed to its conversion to II rather than any direct effect on nucleic acid synthesis (3, 4). Although incubation of I with Ehrlich ascites carcinoma cells demonstrated very little uptake of I, significant intracellular concentrations of II were nonetheless observed (5).

Intravenous doses of I are primarily excreted unchanged in urine together with II and its inactive metabolite, 1-β-D-arabinosyluracil (III) (3, 6, 7). The efficacy of II is limited by its rapid deamination to III (6). It has been suggested that a depot form of II might be useful in maintaining effective levels (8).

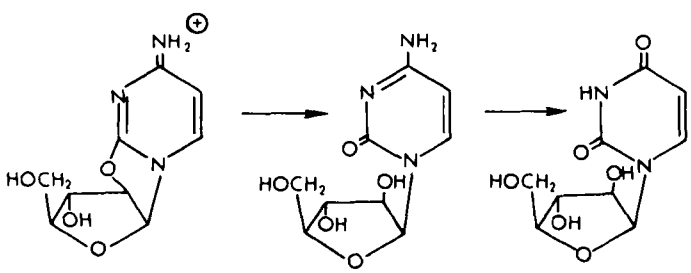

I II III

Scheme I

Unlike II, I is not phosphorylated nor deaminated (6, 9, 10). A prodrug may extend the biological duration of the drug through slow prodrug absorption or rate-limiting conversion to the drug (11). Ancitabine may act as a reservoir through hydrolytic production of II (8).

In vivo conversion of I is thought to be chemical rather than enzymatic hydrolysis (8, 12, 13). The purpose of this study was to investigate the kinetics and mechanisms of prodrug hydrolysis in aqueous solutions. Since I, like II, is not orally active (6), it is important to define its stability for preparation and storage of parenteral formulations.

EXPERIMENTAL SECTION

Stability in Sodium Hydroxide and Hydrochloric Acid Solutions Using Thin-Layer Chromatography—Samples of 0.01 M ancitabine (I)[1] in 0.1 M HCl and 0.05 M NaOH at 50°C were taken over a 4-d period, and 10-μL aliquots were spotted together with reference samples of I, II[2], III[3], and cyclouridine[4] on 20 × 20-cm TLC plates (0.25 mm silica gel GF)[5]. The plates were developed to 10 cm in water-saturated 1-butanol–propanol (3:1), air dried, and examined at 254 nm. A time zero plate was also impregnated with I_2 vapor, and 0- and 1-h plates were sprayed with sulfuric acid and heated. This procedure was also used periodically in the kinetic studies to identify the components in the reaction mixtures.

Spectrophotometric Analysis of Ancitabine and Cytarabine in Mixtures—Absorbance spectra from 220 to 330 nm were obtained for synthetic mixtures to determine which wavelengths could best be monitored for reaction time-course changes[6]. These showed an isosbestic point at 267 nm.

Beer's law plots in 0.1 M HCl provided molar absorptivities (ε) at 240 and 290 nm of 7.25×10^3 and 4.70×10^2 for I and 1.38×10^3 and 1.05×10^4 for II. Known concentrations in mixtures were successfully calculated using:

$$10^5 \cdot [I] = 13.914A_{240} - 1.828A_{290} \quad \text{(Eq. 1)}$$

$$10^5 \cdot [II] = 9.604A_{290} - 0.623A_{240} \quad \text{(Eq. 2)}$$

which were derived from simultaneous equations for total absorbance, A, at 240 and 290 nm for mixtures of I and II.

Analysis of Three-Component Mixtures—Reverse-phase HPLC with

[1] 2,2′-Anhydro-(1-β-D-arabinofuranosyl)-cytosine; Sigma Chemical Co., St. Louis, Mo.
[2] Cytarabine; The Upjohn Co., Kalamazoo, Mich. The chemical name is 1-β-D-arabinofuranosylcytosine, the IUPAC name is arabinosylcytosine, and the common name is cytosine arabinoside (ara-C).
[3] Uracil-β-D-arabinofuranoside; Sigma Chemical Co., St. Louis, Mo.
[4] β-D-O^2,2′-cyclouridine; Terra-Marine Bioresearch, La Jolla, Calif.
[5] Type TLP 109; New England Nuclear, Boston, Mass.
[6] Model 250 spectrophotometer with model 6051 recorder, model 2451A automatic cell positioner, and model 6047 thermosensor; Gilford Instruments, Oberlin, Ohio.

0022-3549/84/0700-0896$01.00/0

Table I—Experimental Conditions for Kinetics of Ancitabine Hydrolysis

Temp., °C	Components[a]	μ[b]	pH	n[c]
19.5	NaOH	0.005-1.0	10.3[d]	7
21.1	NaOH	0.0003-0.00075	10.3-10.7[d]	5
21.2	NaOD[e]	0.0003	10.3[d]	3
26.4	NaOH	1.00	10.7[d]	2
31.4	Na_2CO_3, $NaHCO_3$	1.0	8.6-9.9	7
40.0	H_3BO_3, NaH_2BO_3	1.0	7.8-10.0	8
50.0	NaH_2PO_4, Na_2HPO_4	0.5-1.5	6.2-7.6	24
60.0	NaH_2PO_4, Na_2HPO_4	1.0	5.2-7.4	19
	H_3BO_3, NaH_2BO_3	0.5-1.0	6.4-9.4	29
	$NaHCO_3$, Na_2CO_3	1.0	8.1-8.4	5
	$(CH_2OH)_3CNH_2$, $(CH_2OH)_3CNH_3^+$	1.0	7.8-8.8	5
	$^+H_3NCH_2CO_2Na$, $H_2NCH_2CO_2Na$	1.0	8.5-9.1	6
	CH_3COOH, CH_3COONa	0.01	3.1-3.9	2
	HCl	0.002-0.02	1.6-2.6	2
70.0	NaH_2PO_4, Na_2HPO_4	1.0	6.4-7.5	5
	HCl	0.02	1.6	1
80.0	NaH_2PO_4, Na_2HPO_4	1.0	6.4-7.4	6
	HCl	0.002-1.00	1.5-2.7	4

[a] All reactions aqueous unless otherwise specified. [b] Adjusted with sodium chloride. [c] Number of rate constants determined. [d] Calculated values. [e] Solvent was D_2O.

254-nm fixed-wavelength detection[7] was used to assay I, II, and III in mixtures. The mobile phase was filtered and deaerated, double-distilled water containing 12% (v/v) methanol[8], 0.01 M acetic acid, 0.01 M sodium acetate, and 0.005 M sodium heptanesulfonate as an ion-pairing agent, at 1.0 mL/min. The capacity factors of I, II, and III were 4.4, 1.8, and 0.52, respectively. The peak height *versus* concentration plots were linear in the 1.0×10^{-5} to 10^{-4} M range for all three compounds. Some analyses were carried out using the HPLC method of Tuncel *et al.* (14), with similar results.

Kinetics in Buffers and in Dilute Hydrochloric Acid—Reaction solutions containing I were prepared at various pH values and temperatures (Table I). Those in the pH range of 5.2-10 were assayed as a function of time by diluting aliquots with an appropriate volume of 0.1 M HCl before employing the spectrophotometric analysis (Eqs. 1 and 2) or the HPLC assay (14). In the pH range of 5.2-6.2, mass balance was confirmed by HPLC analysis of [I], [II], and [III] with time (14). For reactions in the pH range of 6.2-10, mass balance was confirmed by monitoring both the isosbestic point and the percent recovery of [I] and [II] as a function of time.

Reactions in the pH range of 1.5-4 were assayed as a function of time by cooling aliquots and applying the HPLC assay reported herein. The sum of the molar concentrations of I, II, and III did not equal the initial concentration of I, $[I_0]$. Complete conversion of I to II was confirmed by fitting concentration-time profiles of II to a biexponential equation using NONLIN (15), calculating the areas under these curves (AUC), and showing them to be equal to the expected values of $[I_0]/k'$, where k' is the rate constant for loss of II.

Kinetics of hydrolysis of I at 80°C were compared with that of II in 0.01 and 0.001 M HCl and in 0.01 M HCl containing 1.0 M NaCl. Samples were assayed as a function of time using the HPLC assay described herein. The concentration of IV (Scheme II) were determined as a function of time by subtracting the sum of the time-dependent concentrations from the initial concentrations of starting material. The rate constants k_{obs}, k', and k_x were determined by simultaneously fitting a series of differential equations describing the concentration-time courses of I, II, III, and IV in Scheme II.

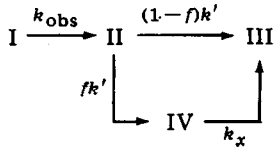

Scheme II

Both k_{obs} and k' were independent of pH and ionic strength in acid. The two pairs of values for k_x provided fractional negative slopes for plots of log k_x *versus* pH or $[\sqrt{\mu}/(1+\sqrt{\mu})]$. Although data are limited, they may indicate that loss of IV may not be a single irreversible process as shown in Scheme II. The value for k' (0.076 h^{-1}) agrees with that previously reported under similar conditions (16).

Kinetics in Dilute Sodium Hydroxide—Distilled-deionized water was refluxed, cooled under nitrogen, and used to prepare solutions containing I in the presence of sodium hydroxide and sodium chloride (Table I). These were maintained at constant temperature under a stream of nitrogen and assayed as a function of time by acidifying aliquots with HCl, measuring absorbances, and applying Eqs. 1 and 2. The influence of ionic strength was quantitated by varying the sodium concentration at 19.5°C (Table II).

***In Situ* Spectrophotometric Analysis of Alkaline Reactions**—Studies for estimating the kinetic isotope effect required the analysis of I and II in reactions carried out in the spectrophotometer using either aqueous sodium hydroxide or sodium deuteroxide in deuterium oxide. Potentiometric titrations of 0.057 M I in 0.05 M HCl with sodium hydroxide showed no evidence for a pK_a. Spectrophotometric data were consistent with this observation. Spectra were superimposable below pH ~8.4. At pH 10.4 and 11.2 absorbance changed with time. The ϵ value at 230 nm, calculated from the intercepts of $\ln(A_t - A_\infty)$ *versus* time, was the same as in acidic solutions.

This pH-independent spectrum for I was compared with that for II in carbonate-free 1×10^{-4} M NaOH. The maximum absorbance differences occurred at 258 and 280 nm. Molar absorptivities (ϵ) at 258 and 280 nm were 1.01×10^4 and 4.69×10^3 for I in double-distilled water and 6.78×10^3 and 7.88×10^3 for II in carbonate-free 1×10^{-4} M NaOH. Concentrations of I and II were calculated from the following equations, derived from simultaneous equations for the total absorbances at 258 and 280 nm:

$$10^4 \cdot [I] = 1.651A_{258} - 1.420A_{280} \quad \text{(Eq. 3)}$$

$$10^4 \cdot [II] = 2.112A_{280} - 0.986A_{258} \quad \text{(Eq. 4)}$$

The accuracy was assumed to be similar to the acid-quenched assay although its assessment using known mixtures under basic conditions was not possible due to the instability of I.

Comparison of Ancitabine Kinetics in Sodium Hydroxide to Those in Sodium Deuteroxide—A closed system with nitrogen-flushed head space was used to limit uptake of atmospheric carbon dioxide and hydrogen-deuterium exchange. Polytef-capped cuvettes were filled with solutions containing either 1.9×10^{-4} M NaOD in deuterium oxide or 1.9×10^{-4} M NaOH in carbonate-free, double-distilled water. Stock solutions of I were prepared free of carbon dioxide and maintained at ambient temperatures. Each reaction in deuterated solvent was duplicated by a corresponding aqueous reaction. An aliquot of the stock solution was quickly added to each cuvette, capped, mixed, and the time of mixing was marked on the recorder[6]. The cuvettes were placed in the thermostated chamber along with a blank. Absorbances of each reaction mixture were automatically recorded at 258 and 280 nm as a function of time using a 2-s dwell time for each cuvette, with automatic reference compensation before and after each reading[6]. Reactions were allowed to proceed until absorbances were constant with time. The temperature in the cuvette chamber was automatically recorded before and after each run. The concentrations of I and II were calculated using Eqs. 3 and 4.

RESULTS

Hydrolysis Products—Reactions monitored by TLC showed I to be stable over a 4-d period at 50°C in water and in 0.1 M HCl, while converting immediately to II in 0.05 M NaOH. At pH ≅ 1.5-6, HPLC analyses detected subsequent deamination of II to III, in accordance with Scheme II. As the pH decreases in this range, the formation of III becomes detectable during the hydrolysis of I because k' passes through a maximum value at pH 3, whereas k_{obs} decreases to a minimum and is constant below pH 4. The AUC values

[7] Model 332 Beckman gradient liquid chromatograph with model 153 analytical detector and Altex ultrasphere-octyl 5-μm column (15 cm × 4.6 mm i.d.); Beckman Instruments, Irvine, Calif.

[8] Omnisolv methanol (glass distilled); MCB Reagents, Norwood, Ohio.

Table II—Selected Experimental Conditions and Rate Constants[a]

Temp., °C	pH	Buffer Concentrations, M		k_{obs}, h^{-1}
		NaH_2PO_4	Na_2HPO_4	
60.0	7.37	0.018	0.180	1.09
	7.25	0.010	0.100	0.816
	7.15	0.005	0.050	0.640
	7.27	0.060	0.300	0.966
	7.17	0.040	0.200	0.750
	7.06	0.025	0.125	0.612
	7.01	0.010	0.050	0.408
	6.98	0.070	0.210	0.540
	6.94	0.050	0.150	0.442
	6.86	0.030	0.090	0.363
	6.80	0.015	0.045	0.294
	6.45	0.250	0.250	0.274
	6.40	0.125	0.125	0.168
	6.33	0.050	0.50	0.122
	6.29	0.025	0.025	0.0935
	5.25	0.500	0.050	0.0354
	5.22	0.250	0.025	0.0232
	5.23	0.100	0.010	0.0182
	5.23	0.050	0.005	0.0152
80.0	6.42	0.200	0.200	2.57
	7.38	0.020	0.200	13.9
	7.08	0.30	0.150	7.86
	6.56	0.100	0.150	2.86
	6.63	0.050	0.100	3.02
	6.42	0.060	0.080	1.92
		$NaHCO_3$	Na_2CO_3	
31.4	9.82	0.060	0.100	4.94
	9.94	0.80	0.160	6.27
	9.61	0.100	0.100	3.07
	9.49	0.130	0.100	2.33
	9.18	0.280	0.100	1.20
	8.89	0.200	0.040	0.661
	8.69	0.450	0.050	0.446
		HCl	μ	
80.0	1.63	0.020	0.02	0.0386
	2.68	0.002	0.002	0.0382
	1.60	0.020	0.100	0.0364
	1.52	0.020	1.000	0.0341
70.0	1.60	0.020	0.02	0.0181
60.0	1.58	0.020	0.02	0.00680
	2.60	0.002	0.002	0.00664
		NaOH		k_{OH}, $10^4(M^{-1}h^{-1})$
19.5	10.44[b]	0.000195	0.005	2.12
	10.43		0.010	2.02
	10.38		0.050	1.68
	10.35		0.100	1.51
	10.32		0.200	1.16
	10.26		0.500	1.04
	10.22		1.000	0.568

[a] The experimental conditions and results presented here are a representative sample of a much larger body of kinetic data. All buffer studies were adjusted to μ = 1.0 using NaCl. [b] Calculated values.

of the concentration–time profiles for II showed that I was quantitatively converted to II. The appearance of an additional, nonchromophoric intermediate in the chemical deamination of II to III, demonstrated previously (16), was confirmed.

Hydrolysis in Acid—In the presence of dilute hydrochloric acid, first-order rate constants $k_s a_{H_2O}$, obtained from linear plots based on:

$$\ln [I] = \ln [I_0] - k_s a_{H_2O} t \qquad \text{(Eq. 5)}$$

were found to be temperature dependent but independent of pH and ionic strength (Fig. 1, Table II).

Hydrolysis in Alkali—In the presence of dilute sodium hydroxide (or deuteroxide), the second-order rate constants, k_{OH}, were obtained from the slopes of linear plots based on:

$$\left\{\frac{1}{[I_0] - [OH_0]}\right\} \cdot \ln \left\{\frac{[I][OH_0]}{[I_0][OH]}\right\} = k_{OH} t \qquad \text{(Eq. 6)}$$

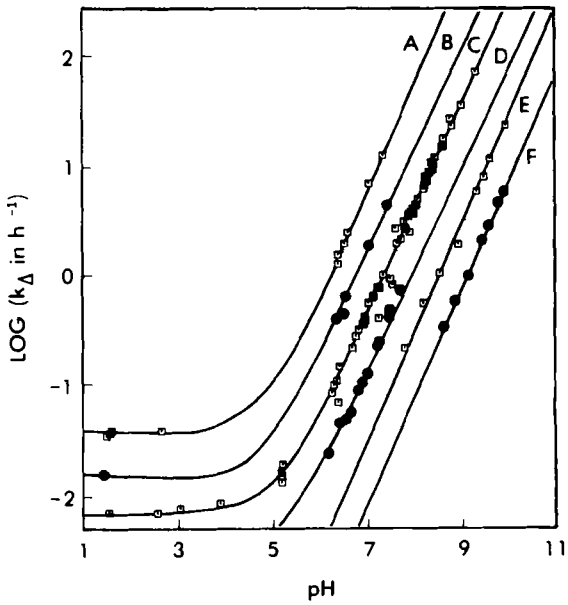

Figure 1—*The pH–rate profile for quantitative conversion of I to II. Data points (k_Δ) represent k_{obs} values corrected for buffer catalysis. Curves are calculated (Eq. 29) at 80°C (A), 70°C (B), 60°C (C), 50°C (D), 40°C (E), and 31.4°C (F). μ = 1.0.*

where [OH] is the concentration of either hydroxide or deuteroxide as determined from $[OH] = [OH_0] - [II]$.

Kinetics in Buffers—In the presence of excess buffer, first-order rate constants (k_{obs}) were obtained from linear plots based on $\ln [I] = \ln [I_0] - k_{obs} t$. Buffer participation was recognized in plots of log k_{obs} *versus* pH, which showed that hydroxide and solvent attack were not sufficient to describe the observed rate constants under all conditions (Fig. 2). General base-catalyzed water attack was hypothesized leading to the overall expression (17):

$$k_{obs} = \left(k^0_{OH}[OH]\frac{\gamma_{OH}\gamma_I}{\gamma_\dagger}\right) + \left(a_{H_2O}\sum_{i=1}^{n} k^0_{B_i}[B_i]\frac{\gamma_I\gamma_{B_i}}{\gamma_{\dagger i}}\right) + (k_s a_{H_2O}) \qquad \text{(Eq. 7)}$$

where k^0_{OH} is the rate constant for hydroxide attack at zero ionic strength, γ_{OH} is the activity coefficient for hydroxide, γ_I is the activity coefficient for I, $\gamma_\dagger$ is activity coefficient for the hydroxide-attack transition state, $[B_i]$ is the concentration of the ith general base, γ_{B_i} is the activity coefficient for the ith base, $\gamma_{\dagger i}$ is the activity coefficient for the transition state for B_i attack, $k^0_{B_i} a_{H_2O}$

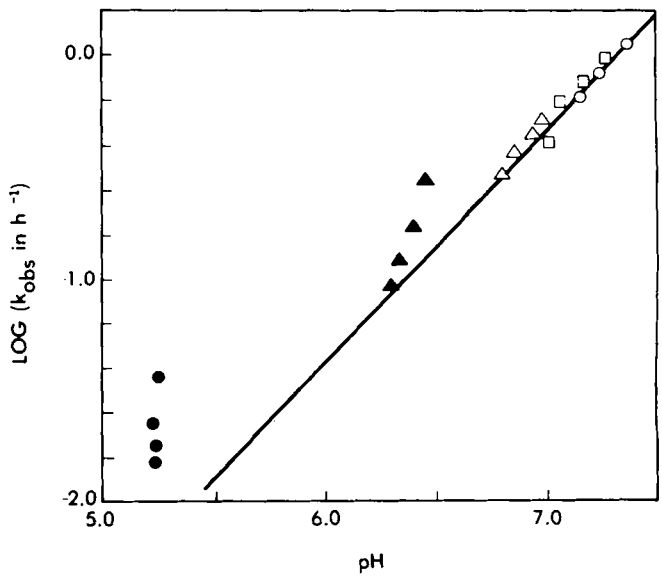

Figure 2—*Log k_{obs} versus pH for quantitative conversion of I to II in phosphate buffers at 60°C, μ = 1.0, where the ratios of $[NaH_2PO_4]/[Na_2HPO_4]$ are: 0.1 (○), 0.2 (□), 0.33 (△), 1.0 (▲), and 10 (●) (see Table II). The regression line, based on the 0.1 ratio buffers (○), has a slope of one.*

Table III—Biomolecular Rate Constants (1/M·h) as a Function of Temperature

Temp., °C	$10^{-5}k^0_{OH}$	$10^{-1}k^0_{cat}$ Phosphate	Borate	Carbonate	
80.0	43.1	5.67	—	—	
70.0	18.5	1.35	—	—	
60.0	7.59	0.444	13.7	88.3	
50.0	4.47	0.115	—	—	
40.0	1.66	—	1.12	—	
31.4	0.779	—	—	1.62	
		Temp., °C	Tris	Glycine	10^2k_s
26.4	0.531	80	—	—	3.84
21.2	0.303	70	—	—	1.81
19.0	0.220	60	0.212	14.3	0.672

equals k^0_{cat}, the bimolecular rate constant for catalysis by the ith base at zero ionic strength, and k_s is the bimolecular rate constant for solvent attack.

Reaction kinetics were studied in solutions of Tris, borate, carbonate, acetate, glycine, and phosphate buffers. Tris, acetate, and borate buffers contained only one Brönsted base species. Although carbonate, glycine, and phosphate buffer contained two general bases, their acids differed by a minimum of four orders of magnitude in K_a values. According to the Brönsted relationship, the efficiency of a general base catalyst increases with the increasing pK_a of its conjugate acid (18). Therefore, the contribution of the more acid base species to k_{obs} was not detectable. The contribution of $k_s a_{H_2O}$ was also insignificant except in buffer solutions of pH ≤5.3. Above this, the observed rate constants in buffers can be described by hydroxide attack plus catalysis by one general base component, B, so that Eq. 7 can be rewritten:

$$k_{obs} = (k^0_{OH} a_{OH} \gamma_I / \gamma_\ddagger) + (k^0_B a_{H_2O} [B] \gamma_B \gamma_I / \gamma_\ddagger') \qquad \text{(Eq. 8)}$$

where $a_{OH} = \gamma_{OH}[OH^-]$ and $k_B{}^0 a_{H_2O} = k_{cat}{}^0$. After taking ionic atmosphere effects into account (see discussion below), observed first-order rate constants were adequately described by this equation. The pH-rate profiles, constructed by subtracting the general base contributions, were linear at pH > 6 with slopes approaching unity, which is the theoretical value when a reaction is first-order in hydroxide (Fig. 1).

Ionic Atmosphere Effects—In dilute hydroxide and buffered solutions, the activity coefficients of the reactants and transition states appear in the rate law for hydrolysis of I. The influence of ionic atmosphere effects on activity coefficients is greater for reactions between ions than for reactions between polar molecules or ions and dipoles (19). Under all conditions studied, I was a cation while hydroxide ion and the general bases (except Tris) were anions.

According to absolute reaction-rate theory, the rate constant is proportional to the concentration equilibrium constant ($k_c^\ddagger$) between the activated complex and the reactants (20). This concentration equilibium constant is affected by the ionic environment and is related to a thermodynamic equilibrium constant ($K_a^\ddagger$) by the ratio of the transition state activity coefficient to the product of the activity coefficients for the reactants (20). For a bimolecular reaction such as the reaction between hydroxide and I:

$$k_{OH} = (k^0_{OH} \gamma_{OH} \gamma_I) \gamma_\ddagger \qquad \text{(Eq. 9)}$$

where k^0_{OH} is the second-order rate constant expressed in terms of the thermodynamic equilibrium constant $K^\ddagger_a$. Carstensen (21) has shown that Eq. 10 adequately describes the logarithm of an activity coefficient based on the kinetic salt effects as reported for the degradation of a number of drugs over a wide range of ionic strengths:

$$\log \gamma_i = \frac{-AZ_i^2\sqrt{\mu}}{1+\sqrt{\mu}} \qquad \text{(Eq. 10)}$$

where γ_i is the activity coefficient of the ith ion, Z_i is its charge, μ is the ionic strength, and A is a function of the temperature and dielectric constant of the solution. According to theory the charge on the transition state is the sum of the charges on the reactants (20). Substitution of Eq. 10 into the logarithmic form of Eq. 9 yields Eq. 11, which predicts a linear relationship between log k_{OH} and $\sqrt{\mu}/(1+\sqrt{\mu})$ with a slope of $-2A$:

$$\log k_{OH} = \log k^0_{OH} - \frac{2A\sqrt{\mu}}{1+\sqrt{\mu}} \qquad \text{(Eq. 11)}$$

This relationship was observed for hydroxide attack on I. Kinetic analyses are more complex in buffers, wherein both primary and secondary salt effects can depend not only on ionic strength but also on specific ionic interactions (22). Activity coefficients of buffer ions can be influenced by the concentration of ions of opposite charge, which often are added as neutral salts to maintain constant ionic strength. This is reflected in the final term of the Guggenheim equation:

$$\log \gamma_i = \frac{-AZ_i^2\sqrt{\mu}}{1+\sqrt{\mu}} + \sum_j \beta_{ij} C_j \qquad \text{(Eq 12)}$$

where β_{ij} represents the interaction coefficients between ion i and all other j ions of opposite charge (20, 22). The activity coefficients in the Henderson-Hasselbach equation:

$$pH = pK_a + \log [B]/[HB] + \log (\gamma_B/\gamma_{HB}) \qquad \text{(Eq. 13)}$$

can be described by Eq. 12 to give:

$$pH = pK_a + \log \frac{[B]}{[HB]} + \frac{(Z_{HB}^2 - Z_B^2)A\sqrt{\mu}}{1+\sqrt{\mu}} + \sum_j \Delta\beta C_j \qquad \text{(Eq. 14)}$$

where HB designates the buffer conjugate acid, $\Delta\beta = \beta_{B_j} - \beta_{HB_j}$, and the summation involves the concentration (C_j) of all the ions of charge opposite to that of buffer ions.

Equation 14 shows that the pH can change as a function of the concentration of ions of charge opposite to that of the buffer ions ($\Sigma_j \Delta\beta C_j$) at constant μ and buffer concentration ratio ([B]/[HB]). For example, the decreasing pH at each constant ($[HPO_4^{2-}]/[H_2PO_4^-]$) ratio observed in Table II is due to increasing sodium ion concentration. In the extreme case, hydroxide activity was observed to decrease from 1.79×10^{-6} to 0.98×10^{-6}, which will have a pronounced effect when hydroxide attack is significant. Therefore, the rate constants for hydrolysis of I in buffers with high concentrations of added neutral salts are not adequately described in terms of concentration.

The following method was developed to solve for the contributions of hydroxide attack and general-base catalysis to the observed first-order rate constants in buffers. Equation 8 was employed to calculate $k_{OH}{}^0$ and $k_{cat}{}^0$ using approximations for $\gamma_\ddagger$, $\gamma_\ddagger'$, and γ_I in the following manner. According to theory the charge on the transition state is the sum of the charges on the species involved in its formation, $Z_\ddagger = Z_A + Z_B + \cdots Z_N$ (20). Therefore, the transition state formed from the hydroxide anion and the I cation was assumed neutral, and its activity coefficient was taken as unity, *i.e.* $\gamma_\ddagger \cong 1$.

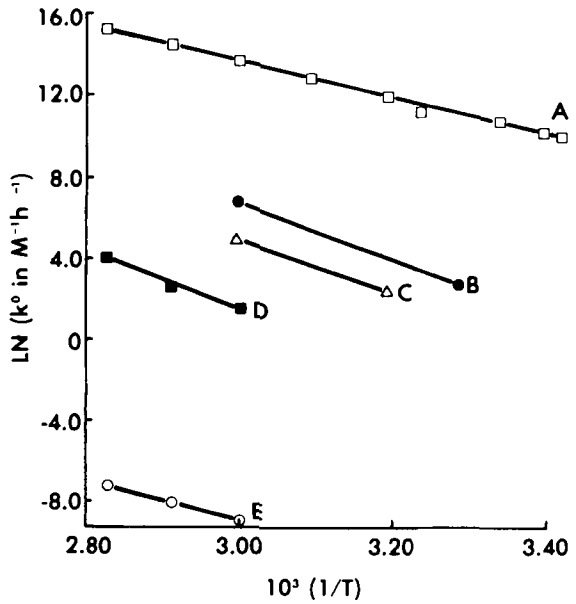

Figure 3—*Arrhenius plots for rate constants at infinite dilution where* k^0 *is* k^0_{OH} *(A),* k^0_{cat} *for carbonate (B), borate (C), and dibasic phosphate (D), and* k_s *(E).*

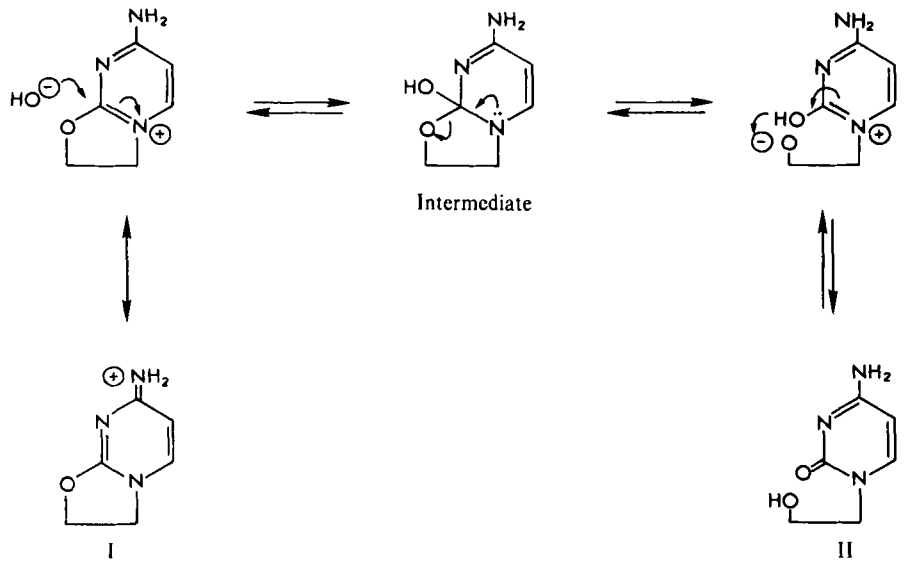

Scheme III

Table IV—Energetics of I Hydrolysis

Rate Constant $M^{-1}h^{-1}$	E_a, kcal/mol-deg	A, $M^{-1}h^{-1}$ [a]	$\Delta H^{\ddagger}$ (kcal/mol-deg) Obs.[a]	Calc.[b]	$\Delta S^{\ddagger}$, e.u.[c]
k^0_{OH}	17.21	1.74×10^{17}	16.6	—	18.0
k^0_{cat}					
Phosphate	29.84	1.45×10^{20}	29.2	29.2	23.6
Carbonate	28.26	2.96×10^{21}	27.2	26.9	28.2
Borate	26.00	1.51×10^{19}	25.4	26.7	17.7
k_s	20.11	2.02×10^{9}	19.4	—	−10.6

[a] Values were calculated at each temperature studied using Eq. 21; the mean values are tabulated. [b] Values were calculated at each temperature studied using Eq. 22 where ΔH^0_{HB} and $\Delta H^0_{H_2O}$ were calculated from literature equations (24). The mean values are tabulated. [c] Values were calculated at each temperature studied using literature equations (25); the mean values are tabulated.

General base-assisted water attack on I would produce the same net charge as protonation of the base to form its conjugate acid, $Z_{\ddagger}' = Z_{HB}$. On this basis, it was assumed that the activity coefficients of these transition states and their corresponding buffer conjugate acids were sufficiently similar to use the approximation $\gamma_{\ddagger}' \cong \gamma_{HB}$. Substitution into Eq. 8 yields:

$$k_{obs} = (k^0_{OH} a_{OH} \gamma_I) + (k^0_B a_{H_2O} [B] \gamma_B \gamma_I / \gamma_{HB}) \qquad \text{(Eq. 15)}$$

Substituting $(K_w[B]\gamma_B/K_a[HB]\gamma_{HB})$ for a_{OH} and dividing the equation by $([B]\gamma_B/\gamma_{HB})$ provides:

$$\frac{k_{obs}}{[B]\gamma_B/\gamma_{HB}} = \left\{\frac{k^0_{OH}\gamma_I K_w}{K_a}\right\} \frac{1}{[HB]} + k^0_B \gamma_I a_{H_2O} \qquad \text{(Eq. 16)}$$

The buffer activity coefficient ratio, γ_B/γ_{HB}, was calculated from pH measurements, known buffer concentrations, and literature values for K_a using:

$$(\gamma_B/\gamma_{HB}) = K_a[HB]/[B]10^{-pH} \qquad \text{(Eq. 17)}$$

which is a rearrangement of the antilogarithmic form of Eq. 13.

Plots of $k_{obs}/([B]\gamma_B/\gamma_{HB})$ *versus* $1/[HB]$ were linear ($r^2 \geq 0.994$) with intercepts of $k_B{}^0\gamma_I a_{H_2O}$ and slopes which allowed the calculation of $k_{OH}{}^0\gamma_I$ after substituting for K_w and K_a. Borate buffers gave the poorest reproducibility ($r^2 = 0.985$), which was probably due to borate polymerization (23) making the true B and HB concentrations unknown.

While Eq. 16 corrects for secondary ionic atmosphere effects, γ_I (a multiplier of both the slope and intercept) is subject to primary salt effects, which are influenced by both ionic strength and specific ionic interactions. The importance of specific ionic interactions appear minor judging from the large r^2 values for each series of buffers at constant ionic strength but varying ion concentrations. To determine the effect of ionic strength on γ_I, a series of 22 reactions were studied in phosphate buffers at 50°C and $\mu = 0.05, 0.20, 0.50$, and 1.00. All reactions were described by a single linear plot ($r^2 = 0.995$) based on:

$$\frac{k_{obs}}{[B]\gamma_B\gamma_I/\gamma_{HB}} = \left\{\frac{k^0_{OH}K_w}{K_a}\right\} \frac{1}{[HB]} + k^0_B a_{H_2O} \qquad \text{(Eq. 18)}$$

since γ_I values were estimated by Eq. 10.

Temperature Dependence—From values of $k^0_{OH}\gamma_I$ and $k^0_{cat}\gamma_I$ obtained in buffers at various temperatures (Eq. 16) and the estimates for γ_I (Eq. 10), k^0_{OH} and k^0_{cat} were calculated at each temperature. Additional k^0_{OH} values were calculated from dilute hydroxide reactions using Eq. 11. Where k_{obs} (*i.e.*, $k_s a_{H_2O}$) values were independent of pH and ionic strength in hydrochloric acid, k_s values were calculated from k_{obs}/a_{H_2O} (Table III). The Arrhenius relationship:

$$\ln k = \ln \underline{A} - E_a/RT \qquad \text{(Eq. 19)}$$

was used to determine the temperature dependence of k^0_{OH}, k^0_s, and k^0_{cat}, where E_a is the activation energy, $\underline{A}$ is the preexponential constant, R is the molar gas constant, and T is the absolute temperature (Fig. 3). The activation energies are given in Table IV.

General Base Catalysis—At 60°C and $\mu = 1.0$, a series of buffers were studied and a Brönsted linear-free energy correlation was demonstrated using:

$$\log\left(\frac{k}{q}\right) = \log G_B + \beta(pK_a + \log p/q) \qquad \text{(Eq. 20)}$$

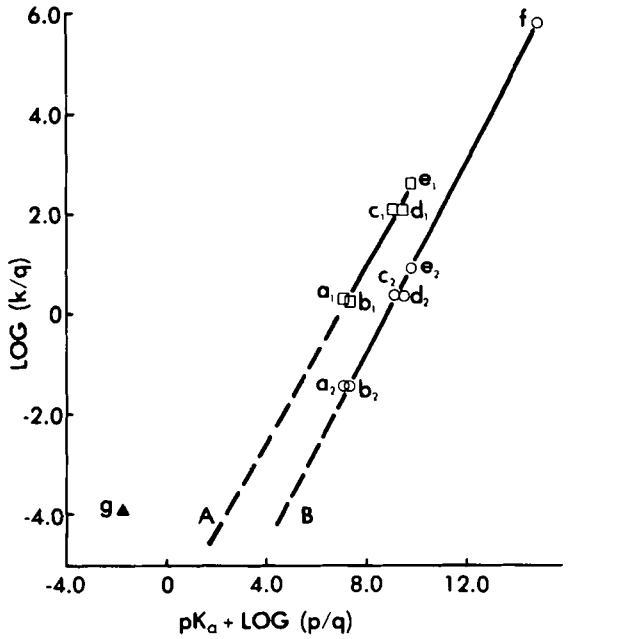

Figure 4—*Brönsted plot relating the rate constants at 60°C for general-base, specific-base, and solvent attack at infinite dilution to the dissociation constants of their conjugate acids (24). Data points represent phosphate (a), Tris (b), glycine (c), borate (d), carbonate (e), k^0_{OH} (f), and k_s (g). Buffer values with subscript 1 (A) represent k^0_{cat}, whereas those with subscript 2 (B) are the corresponding ($k^0_{cat}/55.5$) values. The slopes are 0.90 ($r^2 = 0.95$) for line A and 0.97 ($r^2 = 0.98$) for B.*

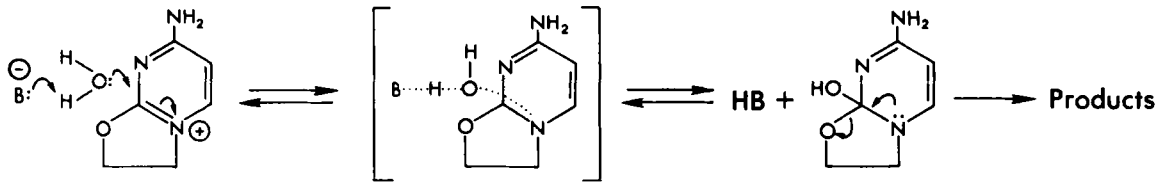

I Intermediate

Scheme IV

where k is the bimolecular rate constant (k^0_{cat}, k_s, or k^0_{OH}), G_B is a constant, β is the Brönsted coefficient, p is the number of equivalent protons which can be transferred from the conjugate acid, and q is the number of sites on the general base which can accept a proton (25). The catalytic constants for general base attack, $k^0_{cat} = k^0_B a_{H_2O}$, were calculated from plots based on Eq. 16 and comprise correlation line A in Fig. 4. As is often observed (18, 26), k^0_{OH} shows negative deviation from the plot and k_s does not fall on the line. Line B is composed of the k^0_{OH} value and those for $k^0_{cat}/55.5$. The agreement between the factor 55.5 and the molarity of pure water may be significant or fortuitous. However, this relationship (line B) will be employed to develop a predictive equation for k_{obs}.

Isotope Effect in the Hydroxide Attack of I—Studies conducted simultaneously in sodium hydroxide and sodium deuteroxide solutions yielded ratios of k^0_{OD}/k^0_{OH} which varied from 0.8 to 1.4. Thus, no significant isotope effect was observed.

DISCUSSION

Mechanism of Hydroxide Attack: Nucleophilic Addition—Scheme III illustrates nucleophilic attack of hydroxide anion at the C-2 position of I, with rate-determining formation of a C—O bond and simultaneous loss of the positive charge to form the tetrahedral intermediate. Subsequent loss of this intermediate could take place as depicted or with general-base assisted transfer of the C-2 hydroxyl proton. Rate-determining formation of the intermediate is consistent with the absence of a significant deuterium isotope effect. Simultaneous loss of the positive charge is supported by a negative ionic strength effect and a positive entropy of activation (Table IV), which is common for reactions in which charge is destroyed in polar media (25).

Mechanism of Buffer Attack: General-Base Assisted Solvent Attack—According to Scheme IV, protonation of the general base, ionization of a water, and formation of the tetrahedral intermediate occur during or prior to the rate-determining step. This is consistent with the observed linear free energy correlation, which includes both hydroxide and general-base assisted solvent attack together with a Brönsted coefficient of unity (Fig. 4). The Brönsted correlation implies that proton transfer is involved at the rate-determining step, and the coefficient value of unity implies that proton abstraction is nearly complete in the transition state (18, 26).

Confirmatory evidence for Scheme IV can be obtained from the activation energies for the rate constants (k^0_{OH} and k^0_{cat}). The enthalpies of activation can be calculated using (26):

$$\Delta H^{\dagger} = E_a - RT \qquad \text{(Eq. 21)}$$

The enthalpy of activation for general base-assisted solvent attack ($\Delta H_B^{\dagger}$), was calculated in two ways. In addition to employing the activation energy in Eq. 21, $\Delta H_B^{\dagger}$ was approximated by:

$$\Delta H_B^{\dagger} = \Delta H_{OH}^{\dagger} + \Delta H^0_{H_2O} - \Delta H^0_{HB} \qquad \text{(Eq. 22)}$$

based on Scheme IV where $\Delta H_{OH}^{\dagger}$ is enthalpy for the formation of the C—O bond calculated from the activation energy of hydroxide attack and Eq. 21, $\Delta H^0_{H_2O}$ is the enthalpy for ionization of water, and ΔH^0_{HB} is the enthalpy for ionization of the conjugate acid (therefore, it is equal to the negative enthalpy of general base-protonation process). There is excellent agreement between the values of $\Delta H_B^{\dagger}$ computed under the assumptions of Scheme IV and those values calculated directly from the experimentally observed activation energies (Table IV).

Mechanism of Solvent Attack—Scheme V depicts a mechanism for solvolysis involving intramolecular general base participation by removal of a proton during nucleophilic attack at C-2. Although there is no direct kinetic support for this anchimeric mechanism, it is consistent with the fact that solvent attack becomes prominent below the reported pK_a (4.2) of II (16) (see Fig. 1). Assuming the ability of the tetrahedral intermediate to accept a proton at N-3 is approximately the same as that of II, Eq. 20 with $pK_a = 4.2$ was used to calculate k^0_{cat}. The ratio of $k_s a_{H_2O}/k^0_{cat}$, which represents the "effective concentration" of intramolecular catalyst in the vicinity of I, was calculated to be 3 M. This value suggests that the intramolecular rate enhancement can be accounted for by local concentration effects (27).

Stability Prediction for Ancitabine Conversion—The rate constant for conversion of I to II was shown to be the sum of the rate constants for water attack (Eq. 5), hydroxide attack, and general base-catalyzed water attack (Eq. 8) and therefore can be defined:

$$k_{obs} = k^0_{OH} a_{OH} \gamma_I + k^0_{cat}[B]\left[\frac{\gamma_B \gamma_I}{\gamma_{HB}}\right] + k_s a_{H_2O} \qquad \text{(Eq. 23)}$$

It was observed that using $k^0_{cat}/55.5$ values resulted in a common Brönsted plot which included the k^0_{OH} value. The agreement between 55.5 and the molecularity of pure water may be coincidental, but the observation was used to derive a predictive equation for k_{obs}. Since $\beta \cong 1$ (line B, Fig. 4) the antilogarithmic form of Eq. 20 may be written:

$$k^0_{OH} = G_B/K'_a \qquad \text{(Eq. 24)}$$

where $p = q = 1$ and $K'_a = K_w/a_{H_2O}$ and:

$$k^0_{cat}/55.5 = G_B p/K_a \qquad \text{(Eq. 25)}$$

Therefore, k^0_{cat} can be described in terms of $k_{OH}{}^0$ as:

$$k^0_{cat} = 55.5 k^0_{OH} K'_a p/K_a \qquad \text{(Eq. 26)}$$

Arrhenius parameters were determined for k^0_{OH} and k_s (Fig. 3, Table IV) from:

$$k^0_{OH} = \underline{A} \cdot \exp(-E_a/RT) \qquad \text{(Eq. 27)}$$

$$k_s = \underline{A}' \cdot \exp(-E_a'/RT) \qquad \text{(Eq. 28)}$$

Substitution for γ_I (Eq. 10), γ_B/γ_{HB} (Eq. 17), k^0_{cat} (Eq. 26), k_s (Eq. 28), and $a_{OH} = K_w 10^{pH}$ into Eq. 23 yields:

$$k_{calc} = (1 + X)\underline{A} a_{OH} \cdot \exp\left(\frac{-2.3A\sqrt{\mu}}{1 + \sqrt{\mu}} - \frac{E_a}{RT}\right) + \underline{A}' a_{H_2O} \cdot \exp\left(-\frac{E_a}{RT}\right) \qquad \text{(Eq. 29)}$$

where a_{OH} is calculated from measured pH and K_w at temperature T. This describes the first-order rate constant for loss of I, k_{calc} in h^{-1}, as a function of pH, ionic strength, and temperature where $X = p \cdot [HB]/1$ M reflects the concentration [HB] and type (p) of the conjugate acid. Figure 5 demonstrates the agreement between rate constants calculated by Eq. 29 (k_{calc}) and those observed in this study (k_{obs}).

Substitution for the constants provides the following:

$$k_{calc}\,(h^{-1}) = (1 + X)1.74 \times 10^{17} a_{OH} \cdot \exp\left(\frac{-1.15\sqrt{\mu}}{1 + \sqrt{\mu}} - \frac{8662}{T}\right) + 1.12 \times 10^{11} \cdot \exp(-10{,}121/T) \qquad \text{(Eq. 30)}$$

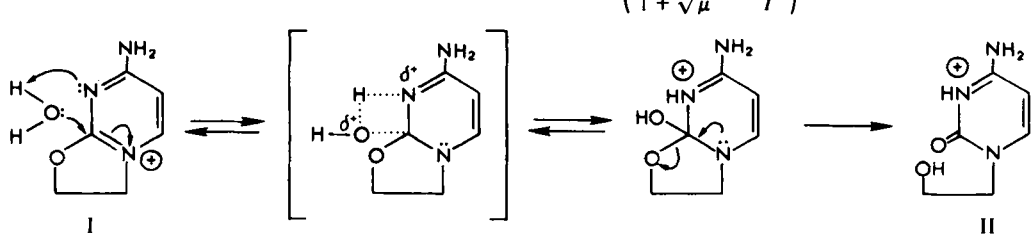

I II

Scheme V

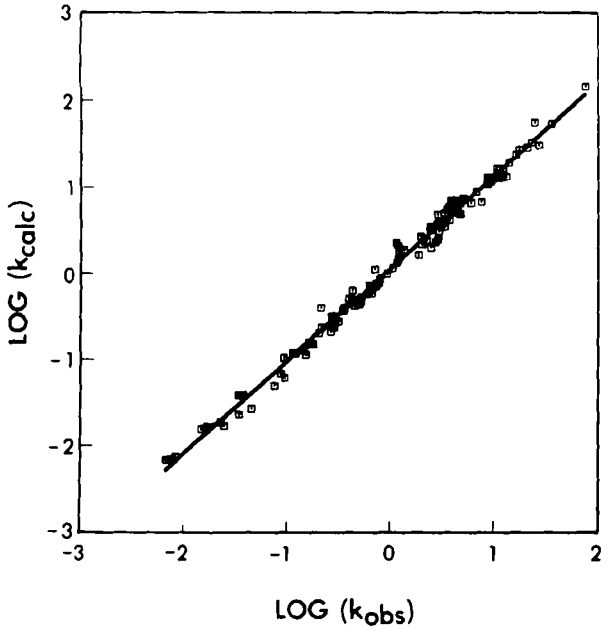

Figure 5—*Correlation between first-order rate constants for conversion of I calculated using Eq. 29 (k_{calc}) and observed (k_{obs}) in 125 reactions in the pH range 1.5–10.7, the temperature range 19.5–80°C; the ionic strength range 1×10^{-4} to 1.5; and in various concentrations of phosphate, borate, glycine, Tris, carbonate, and acetate buffers, hydrochloric acid, and sodium hydroxide solution. These rate constants were plotted* versus *the calculated rate using a log–log scale to facilitate visualization of the entire range of values. The slope of the log–log plot is 1.060 ($r^2 = 0.992$).*

which requires only the measured pH (for a_{OH}), temperature, concentration [HB], and type (p) of conjugate acid to solve for k_{calc}.

REFERENCES

(1) A. Hoshi, F. Kanzawa, and K. Kuretani, *Gann*, **63**, 353 (1972).

(2) J. M. Vanditti, M. C. Baratta, N. Greenberg, B. J. Abbott, and I. Kline, *Cancer Chemother. Rep.*, **56**, 483 (1972).

(3) F. Hamada, T. Sugihara, S. Tsuyama, H. Hirayama, T. Kani, M. Nishimure, L. Kuretani, and A. Hoshi, *Chem. Pharm. Bull.*, **23**, 586 (1975).

(4) A. Hoshi, M. Yoshida, K. Kuretani, T. Kanai, and M. Ichino, *Chem. Pharm. Bull.*, **23**, 1814 (1975).

(5) M. C. Wang, R. A. Sharma, and A. Bloch, *Cancer Res.*, **33**, 1265 (1973).

(6) D. H. W. Ho, C. J. K. Carter, T. L. Loo, R. L. Abbott, and C. M. McBride, *Drug Metab. Dispos.*, **3**, 309 (1975).

(7) D. H. W. Ho, V. Rodriguez, T. L. Loo, G. P. Bodey, and E. J. Freireich, *Clin. Pharmacol. Ther.*, **17**, 66 (1975).

(8) D. H. W. Ho, *Cancer Chemother. Rep.*, **61**, 717 (1977).

(9) A. Hoshi, M. Iigo, M. Saneyoshi, and L. Kuretani, *Chem. Pharm. Bull.*, **21**, 1535 (1973).

(10) W. Kreis, T. M. Woodcock, M. B. Meyers, L. A. Carlevarini, and I. H. Krakoff, *Cancer Chemother. Rep.*, **61**, 723 (1977).

(11) R. E. Notari, *Pharmacol. Ther.*, **14**, 25 (1981).

(12) D. H. W. Ho, *Biochem. Pharmacol.*, **23**, 1235 (1974).

(13) K. J. Himmelstein and J. F. Gross, *J. Pharm. Sci.*, **66**, 1441 (1977).

(14) M. Tuncel, R. E. Notari, and L. Malspeis, *J. Liq. Chromatogr.*, **4**, 887 (1981).

(15) C. M. Metzler, G. L. Elfring, and A. J. McEwen, *Biometrics*, **30**, 3 (1974).

(16) R. E. Notari, M. L. Chin, and R. Wittebort, *J. Pharm. Sci.*, **61**, 1189 (1972).

(17) A. W. Moore and R. G. Pearson, "Kinetics and Mechanisms," 3rd ed., Wiley, New York, N.Y., 1981, pp. 347–353.

(18) T. C. Bruice and S. Benkovic, "Bioorganic Mechanisms," vol. 1, W. A. Benjamin, New York, N.Y., 1966, pp. 27–46.

(19) E. S. Amis and J. F. Hinton, "Solvent Effects on Chemical Phenomena," Academic, New York, N.Y., 1973, chap. 5.

(20) B. Perlmutter-Hayman, *Prog. React. Kinet.*, **6**, 239 (1972).

(21) J. T. Carstensen, *J. Pharm. Sci.*, **59**, 1140 (1970).

(22) A. D. Pethybridge and J. E. Prue, *Prog. Inorg. Chem.* **17**, 327 (1972).

(23) W. P. Jencks, "Catalysis in Chemistry and Enzymology," McGraw-Hill, New York, N.Y., 1969, p. 470.

(24) H. S. Harned and B. B. Owen, "The Physical Chemistry of Electrolytic Solutions," Reinhold, New York, N.Y., 1958, chapt. 15.

(25) F. A. Carey and R. J. Sundberg, "Advanced Organic Chemistry: Part A," Plenum, New York, N.Y., 1977, pp. 137–139.

(26) W. P. Jencks, "Catalysis in Chemistry and Enzymology," McGraw-Hill, New York, N.Y., 1966, pp. 170–181.

(27) W. P. Jencks, "Catalysis in Chemistry and Enzymology," McGraw-Hill, New York, N.Y., 1966, pp. 10–18.

ACKNOWLEDGMENTS

The authors gratefully acknowledge the Elsa U. Pardee Foundation, The National Institutes of Health (Predoctoral Training Grant T32GM07622-05), and The Upjohn Company for partial support of this work.